

Cite this: DOI: 00.0000/xxxxxxxxxx

Dynamics of microstructure anisotropy and rheology of soft jammed suspensions

Nicolas Cuny,^a Eric Bertin,^a and Romain Mari^{*a}Received Date
Accepted Date

DOI: 00.0000/xxxxxxxxxx

We explore the rheology predicted by a recently proposed constitutive model for jammed suspensions of soft elastic particles derived from particle-level dynamics [Cuny *et al.*, Phys. Rev. Lett. **127**, 218003 (2021)]. Our model predicts that the orientation of the anisotropy of the microstructure, governed by an interplay between advection and contact elasticity, plays a key role at yielding and in flow. It generates normal stress differences contributing significantly to the yield criterion and Trouton ratio. It gives rise to non-trivial transients such as stress overshoots in step increases of shear rate, residual stresses after flow cessation and power-law decay of the shear rate in creep. Finally, it explains the collapse of storage modulus as measured in parallel superposition for a yielded suspension.

1 Introduction

Soft jammed suspensions are a class of materials made of soft, elastic particles immersed in a fluid, with a concentration large enough to create a continuous elastic network of contacts, which induces a yield stress. Concentrated suspensions of microgels, concentrated emulsions or wet foams belong to this family¹. Despite being common occurrence in industrial contexts, in particular in the food and cosmetic industries, the rheology of these materials is still being explored, and many open questions remain, not only regarding quantitative characterization, but also regarding what observables are most suited to describe these systems, especially in their yielded phase². The yield point and steady rheology under flow have been the main focus of the literature, and in most cases results concern simple shear, for which only the shear stress is reported.

Based on simple shear results, a qualitative rheological picture for homogeneous flows (which are not always the norm^{3,4}) has emerged. Soft jammed suspensions follow a Herschel-Bulkley rheology with the shear stress σ related to the shear rate $\dot{\gamma}$ as $\sigma = \sigma_{y,s} + k\dot{\gamma}^n$, with $\sigma_{y,s}$ the (simple shear) yield stress, $k > 0$ the consistency parameter and the flow parameter $n \approx 0.5$ ^{3,5–8}. Before this steady-state stress is reached, soft jammed suspensions sometimes exhibit a stress overshoot, that is, a transient maximum before decreasing to the steady-state stress value^{4,9–14}. In contrast, tensorial and temporal aspects only quite recently received some attention^{4,15–17}, despite the importance of the question in virtually any practical application, which involve unsteady conditions and varying flow geometries.

The history of constitutive modelling is consequently equally steady-simple-shear centric. Many phenomenological models are designed around the scalar HB rheology, from which a tensorial extension is postulated^{18–21}. These models involve a von Mises criterion for the yield, based on the second invariant of the deviatoric stress tensor Σ' , stating that yield occurs when $\sqrt{\Sigma' : \Sigma'}/2 = \tau_c$, with τ_c a material property (and therefore independent of the type of deformation under which yield is achieved). The validity of the von Mises yield criterion, as well as the experimental methodologies to test it, have been recently actively debated^{15,22–28}. In particular, there is no consensus as to whether measuring the yield shear stress in a simple shear setup is enough to determine τ_c if the von Mises criterion holds, or equivalently, whether normal stresses at yield under simple shear are negligible in front of the shear stress^{15,27}.

Separately, dynamical aspects of soft jammed suspensions are also poorly understood. Shear under constant imposed stress set at the yield value induces a creep behavior, with a power law decay of the shear rate as a function of time^{3,29}. Flow cessation leads to residual stresses, which amplitude decreases with the stress or rate applied in pre-shear^{16,30,31}. Finally, while viscoelasticity in unsheared materials is well studied, the linear response under flow (often called parallel superposition) shows interesting unexplained features: at fixed frequency the storage modulus strongly decreases as a function of applied stress above yield, while the loss modulus shows a more moderate decay, with a possible upward jump at yielding^{17,32}, suggesting a loss of elastic integrity of the particle contact network which is difficult to reconcile with the picture of densely packed particles above their jamming point.

Using a recent constitutive model derived from particle-level

^a Univ. Grenoble Alpes, CNRS, LIPhy, 38000 Grenoble, France, E-MAIL: romain.mari@univ-grenoble-alpes.fr

dynamics³³, we here address tensorial and dynamical aspects of the rheology of soft jammed suspensions, namely the contribution of normal stresses to the von Mises criterion and Trouton ratio under flow, the linear response under shear, and the transients under step changes in applied stress or rate. Thanks to the microscopic grounding of our model, we can relate the rheology to microstructure evolution. We will see that in many cases, the tensorial nature of the anisotropy of the elastic contact network, which couples to the vorticity when straining is present, plays a simple but central role in apparently complex rheological responses. The tensorial elasticity/advection interplay is particularly simple in slow flows, that is, those for which the deformation rate is small in front of the inverse elastic timescale. For these, the total stress is essentially coming from the elastic particle stress. We show that the amplitude of the deviatoric stress relaxes elastically, and thus has a much faster dynamics than the orientation of its principal axes, which is advected. We find that this amplitude/orientation timescale decoupling is leading to possibly deceiving transient behaviors for the shear component of the stress in simple shear. More generally, for flows with both finite strain and finite vorticity, one needs to acknowledge the presence of normal stress differences to build a coherent physical picture.

2 Constitutive model

2.1 Stress evolution

In a recent work^{33,34}, we derived from microscopic dynamics a constitutive law for a two-dimensional system of overdamped frictionless harmonic disks above the jamming transition. This system is an idealized model for soft jammed suspensions such as concentrated emulsions or microgels^{8,35–37}. In this model, disks of radius a interact through radial contact repulsion forces deriving from the harmonic potential $V(r) = af_0(1 - r/2a)^2\Theta(1 - r/2a)$ with Θ the Heaviside function. They are further subject to a viscous drag $-\lambda_f(\dot{\mathbf{r}}_i - \mathbf{u}^\infty(\mathbf{r}_i))$, where $\dot{\mathbf{r}}_i$ is the velocity of particle i , and $\mathbf{u}^\infty(\mathbf{r}_i)$ the velocity at the particle position of a fictitious fluid that induces shear in the system. This model is characterized by an elastic timescale $\tau_0 \equiv f_0/(\lambda_f a)$.

Under a uniform applied flow, characterized by its velocity gradient $\nabla\mathbf{u}^\infty$ (which we define as $(\nabla\mathbf{u}^\infty)_{ij} = \partial_j u_i^\infty$), there is a regime, away from jamming and yielding criticalities, for which flow is homogeneous in space and time. This stands in contrast to the plastic-event dominated regime close to the yielding transition³⁸, and the soft-mode dominated regime close to jamming³⁹. In Refs.^{33,34}, we derived in this regime the following evolution equation for the deviatoric part of the particle (or elastic) stress tensor Σ'

$$\dot{\Sigma}' = \kappa(\phi)\mathbf{E}^\infty + \mathbf{\Omega}^\infty \cdot \Sigma' - \Sigma' \cdot \mathbf{\Omega}^\infty + [\beta(\phi) - \xi(\phi)(\Sigma' : \Sigma')] \Sigma', \quad (1)$$

where the strain-rate tensor \mathbf{E}^∞ and the vorticity tensor $\mathbf{\Omega}^\infty$ are respectively the symmetric and antisymmetric parts of $\nabla\mathbf{u}^\infty$. The coefficients κ , β and ξ have known expressions as a function of the area fraction ϕ and of particle-level parameters. The key steps of the derivation are recalled in Appendix A. In short, the basic idea is to derive an evolution equation for the stress tensor from the evolution equation of the pair correlation function (the athermal

equivalent of the Smoluchowski equation^{40–43}), using the virial definition of the stress to relate microstructure to stress. A set of physically plausible approximations then allows one to get the closed evolution equation Eq. (1) for the deviatoric part Σ' of the particle stress tensor. This stress evolution focuses on the regime where the total stress is mostly coming from the elastic forces, rather than viscous dissipation, that is, for $\dot{\gamma} \equiv \sqrt{2\mathbf{E}^\infty : \mathbf{E}^\infty} \ll \tau_0^{-1}$ (small Weissenberg numbers). We stress here that Eqn (1) is for a two-dimensional system, for which the usual advection term proportional to $\mathbf{E}^\infty \cdot \Sigma' + \Sigma' \cdot \mathbf{E}^\infty$ has vanishing deviatoric contribution.

This constitutive model is formally quite similar to the Saramito model¹⁹ above yield, except that our microscopic derivation leaves no freedom to the parameters, which are entirely determined from microscopic properties. Indeed, the parameters κ , β and ξ are known analytical functions (albeit complicated ones) of the area fraction ϕ of the suspension. Note that dimensional analysis imposes that they also are functions of the particle radius and stiffness and of the fluid viscosity as $\kappa \propto f_0/a = \lambda_f \tau_0$, $\beta \propto \tau_0^{-1}$ and $\xi \propto a^2/(\tau_0 f_0^2) = 1/(\lambda_f^2 \tau_0^3)$. Linearizing these functions at the jamming transition located at ϕ_J , we find $\kappa a/f_0 \approx 1.19 - 0.099\Delta\phi$, $\beta \tau_0 \approx 0.16 + 0.76\Delta\phi$, and $\xi \tau_0 f_0^2/a^2 \approx 0.62 + 0.0054\Delta\phi$, with $\Delta\phi = \phi - \phi_J$. As the approximations involved in deriving Eqn (1) assume that we are not very close to jamming, these expressions should be taken as approximations rather than controlled perturbative expansions around jamming.

In spite of the interest of having a microscopically grounded constitutive model, a possible drawback is that the model has no fitting flexibility, and its quantitative predictions depend on the details of the quality of the closures used in the derivation. For instance, it predicts a yield stress³³ for volume fractions larger than a jamming volume fraction $\phi_J = 1.25$, which is around 50 % larger than the actual measured values in simulations³⁵. Finally, this model is for uniformly flowing suspensions. It does not possess an elastic branch before yield, nor even a static mechanical equilibrium inside the yield surface. Furthermore, because it does not consider spatial and temporal fluctuations like plastic events, it predicts a Bingham rheology³³, as opposed to a Herschel-Bulkley one with $n < 1$.

Nonetheless, our model is the first one to explicitly associate a microscopic picture with the macroscopic rheology of concentrated suspensions of elastic particles. It thus provides a frame of thought to approach these systems, with clearly stated organizing principles, such as the microstructure-stress relation we present below, which strengths and weaknesses can be discussed.

2.2 Characterizing generic steady uniform flows

In this article, we will study in depth tensorial aspects of our model, testing in particular its dependence on flow geometry. For this, it is useful to define the entire set of possible steady uniform flow geometries in two dimensions. For a given steady uniform flow defined by its velocity gradient $\nabla\mathbf{u}^\infty$, we call flow geometry (or “shape”) the tensor $\mathbf{K}^\infty = \nabla\mathbf{u}^\infty/\sqrt{\nabla\mathbf{u}^\infty : \nabla\mathbf{u}^\infty}$. (This definition of \mathbf{K}^∞ is a special case of the more general, frame-indifferent definition used for arbitrary unsteady and non-uniform flows, that we give in Appendix B.) While in two dimensions $\nabla\mathbf{u}^\infty$ has three in-

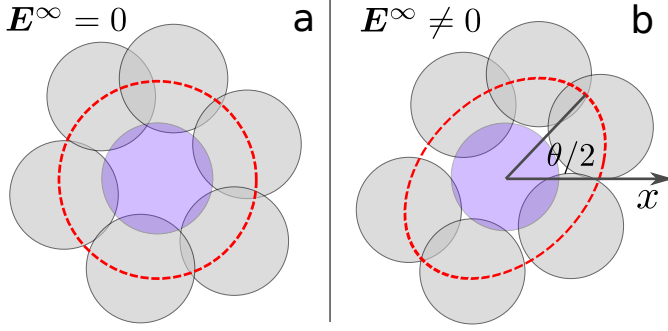


Fig. 1 (a) A soft jammed suspension in isotropic conditions, without externally applied deformation. The central particle is surrounded by a shell of nearest neighbors which centers are located near the red dashed line. (b) Under an applied strain rate, the microstructure develops an anisotropy, here represented by the deformation of the initially circular nearest-neighbor peak location. The anisotropy is characterized by an amplitude S (see main text for definition) and an orientation $\theta/2$ of its main axis with respect to the x direction.

dependent values, the flow geometry, being the normalized $\nabla \mathbf{u}^\infty$, has only two. Moreover, because all flow geometries differing only by a solid rotation are equivalent, we can without loss of generality restrict our exploration to a one-dimensional family parametrized by a single angle $\alpha \in [0, \pi/2]$,

$$\mathbf{K}^\infty = \frac{1}{\sqrt{2}} \begin{pmatrix} \cos \alpha \cos 2\alpha & 2 \sin \alpha + \sin \alpha \cos 2\alpha \\ \sin \alpha \cos 2\alpha & -\cos \alpha \cos 2\alpha \end{pmatrix}. \quad (2)$$

Planar extensional flow corresponds to $\alpha = 0$, simple shear is obtained for $\alpha = \pi/4$, while for $\alpha = \pi/2$ the flow is purely rotational (and thus no yield is possible for this value). The derivation of Eqn (2) is given in Appendix B.

2.3 Microstructure-stress relation

We will exploit the microscopic grounding of the model in order to relate rheological features to microstructural ones at the level of the pair correlation function $g(\mathbf{r})$ between particles. Indeed, in our model we find that the deviatoric stress Σ' is proportional to the fabric tensor \mathbf{Q} , $\Sigma' = \mu(\phi)\mathbf{Q}$. This tensor encodes the lowest order in anisotropy of the pair correlation function³⁴, and is defined as

$$\mathbf{Q} = \frac{\phi^2}{2\pi^2 a^4} \int_{|\mathbf{r}| \leq 2a} \left[\mathbf{r} \otimes \mathbf{r} - \frac{|\mathbf{r}|^2}{2} \mathbf{1} \right] g(\mathbf{r}) d\mathbf{r}. \quad (3)$$

\mathbf{Q} is traceless, so it has two eigenvalues equal in amplitude but of opposite signs. The eigenvector with positive eigenvalue λ (resp. negative eigenvalue $-\lambda$) corresponds to the direction where particle contacts are the least (resp. the most) compressed under flow, as depicted in Fig. 1b. In this figure we defined as $\theta/2$ the angle that the eigenvector with positive eigenvalue makes with the x direction.

Because $\Sigma' = \mu(\phi)\mathbf{Q}$, θ also quantifies the tilt of the stress anisotropy, and Σ' takes the form

$$\Sigma' = S \begin{pmatrix} \cos \theta & \sin \theta \\ \sin \theta & -\cos \theta \end{pmatrix}, \quad (4)$$

where we define S as the amplitude of the stress anisotropy. The pair (S, θ) is the polar coordinate system associated with the deviatoric stress tensor, and is related to the usual viscometric functions as $\sigma \equiv \Sigma'_{xy} = S \sin \theta$ and $N_1 \equiv \Sigma'_{xx} - \Sigma'_{yy} = 2S \cos \theta$.

The major advantage of the polar representation is that it decouples the role of the two competing processes at stake, namely elastic relaxation and advection. Indeed, the amplitude of the microstructure anisotropy S/μ relaxes elastically, with a typical timescale τ_0 , while the tilt $\theta/2$ evolves only under advection, with a typical timescale $\dot{\gamma}^{-1}$. In the elastically dominated flow regime $\dot{\gamma}\tau_0 \ll 1$ we consider here, it results in a separation of timescales: S is a fast variable, θ a slow one.

A final remark here is that if $\theta = 2\alpha$, that is, Σ' aligned with \mathbf{E}^∞ , the most (respectively least) compressed contacts are along the compressional (resp. elongational) direction of flow. As we will see, the stress evolution in Eqn (1) is such that in practice, for $0 < \alpha < \pi/2$, the vorticity rotates the microstructure and therefore misaligns it with respect to \mathbf{E}^∞ (i.e. $\theta \neq 2\alpha$). This simple mechanism is giving rise to most of the rheological phenomena discussed in this work.

3 Dependence on flow geometry

3.1 Yield: von Mises criterion

The question of the yield of soft jammed suspensions (and yield stress fluids in general⁴⁴) in arbitrary geometries has recently seen a surge of activity^{15,26–28}. This renewed interest stems from the development of new experimental techniques to measure the relevant stress components at yield in extensional flows^{26,44}. Indeed, historically the yield shear stress under simple shear has been by far the most commonly measured yield stress, and served as a reference point for the development of constitutive models.

The motivation to compare the yield in extension and simple shear flows revolves around two questions: (i) the validity of the so-called von Mises criterion, which states that under an arbitrary deformation, yield occurs when $\sqrt{\Sigma' : \Sigma'}/2 = \tau_c$, with τ_c a geometry independent “yield” stress, and (ii) the weight of normal stress differences under simple shear in the von Mises criterion if it applies²⁷. Both issues remain unresolved, with experiments showing apparently contradicting results. Some experiments find a good agreement with the von Mises criterion^{15,22,24} while others do not^{26,28}. However in many works normal stress differences in simple shear are assumed to vanish, which is debated^{27,28}.

In our constitutive model, Eqn (1), the von Mises criterion naturally holds, with $\tau_c(\phi) = \sqrt{\beta(\phi)/2\xi(\phi)}$. It shares this property with phenomenological models^{18–20,45,46}, while in MCT-ITT for soft glasses deviations from the von Mises criterion are tiny, despite the criterion not being baked in⁴⁷.

We have already shown that in simple shear, our model predicts that at yield the normal stress difference is larger in magnitude than the shear stress³³. The contribution of normal stresses to the yield criterion thus cannot be neglected, which is consistent with some^{26,28}, but not all¹⁵ experimental observations. We here report the evolution of the relative contributions of shear and normal stresses to the von Mises criterion by exploring the entire family of possible flows for our constitutive model, given

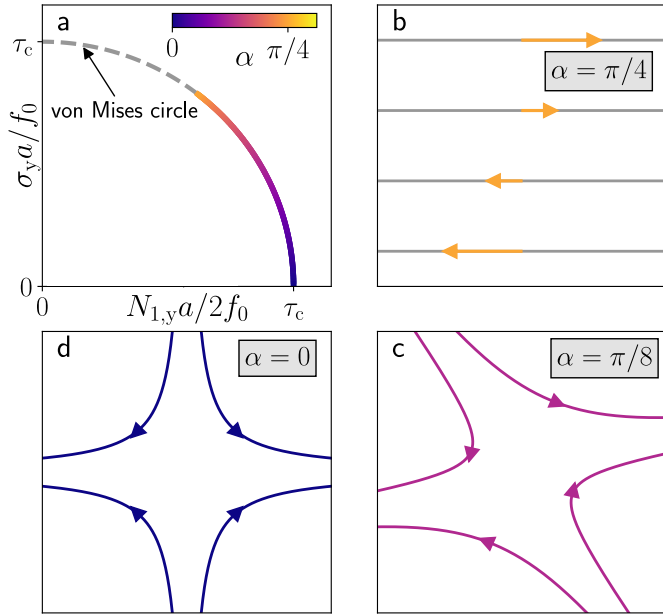


Fig. 2 (a) The von Mises criterion (dashed gray line) in our model. For two-dimensional flows (parametrized by the angle α as defined in Eqn (2)), the dynamic yield stress is unique to each flow geometry, as shown in colored line. (b)–(d) Different flows in the family, in clockwise order $\alpha = \pi/4$ (b, simple shear), $\alpha = \pi/8$ (c) and $\alpha = 0$ (d, planar extensional).

by Eqn (2).

For a two-dimensional system, the von Mises criterion states that yield occurs on a circle of radius τ_c in the plane $(N_1/2, \sigma)$, represented in Fig. 2a for $\phi = 1.26$. In our model, the degeneracy is lifted only for the dynamic yield stress tensor by taking the solution of Eqn (1) in the $\dot{\gamma} \rightarrow 0$ limit. We thus here focus on the dynamic yield stress. Defining the angle θ_y separating the yield point from the $N_1/2$ axis, we have

$$\theta_y = 2\alpha - \arcsin \left[\frac{2\tau_c(\phi) \tan \alpha}{\kappa(\phi)} \right]. \quad (5)$$

This admits solutions only when $\alpha \in [0, \arctan\{\kappa(\phi)/2\tau_c(\phi)\}]$. For larger values of α , corresponding to flows mostly (but not purely) rotational, our constitutive equation admits no steady solution under flow, instead the stress tensor keeps rotating with the applied flow. We represented the solution in Fig. 2a, along with some of the corresponding flows in panels (b)–(d).

Because $\theta_y < \pi/2$ for all α values, normal stresses always have a significant contribution to the von Mises criterion. This in particular points to the importance of measuring normal stresses at yield under simple shear for soft jammed suspensions²⁷. Furthermore, in a three-dimensional system, a finite second normal stress difference would presumably also contribute to the von Mises criterion.

At the microstructure level, normal stresses in simple shear stem from the misalignment of the principal axes of the fabric tensor \mathbf{Q} with the ones of the symmetrized strain rate tensor \mathbf{E}^∞ . Due to the vorticity of the flow, the most compressed contacts lie between the compression and flow gradient directions. In conse-

quence, the largest contact forces have a larger projection on the flow gradient direction than on the flow direction, which leads to $N_1 > 0$.

This challenges the common assumption that the deviatoric stress is quasi-Newtonian^{22,26,48–50}. The main corollary of this assumption is that the sole (or at least the main¹⁵) contributor to the von Mises criterion is the projection of the deviatoric stress tensor on \mathbf{E}^∞ , i.e. $\boldsymbol{\Sigma}' : \mathbf{E}^\infty / \sqrt{2\mathbf{E}^\infty : \mathbf{E}^\infty}$ ²². Our constitutive model shows that this assumption is likely not verified in most flows except the most extensional ones. As soon as the vorticity tilts \mathbf{Q} (and thus $\boldsymbol{\Sigma}'$) by an angle ν with respect to \mathbf{E}^∞ , the component of $\boldsymbol{\Sigma}'$ tensorially orthogonal to \mathbf{E}^∞ starts to contribute to $\boldsymbol{\Sigma}' : \boldsymbol{\Sigma}'$. For small ν , this contribution is quadratic, but already for $\nu \approx 9^\circ$ it accounts for 10% of $\boldsymbol{\Sigma}' : \boldsymbol{\Sigma}'$, and for $\nu \approx 22^\circ$ it reaches 50%.

The role of the vorticity in a stress evolution such as Eqn (1) is constrained by frame indifference for inertialess systems⁵¹. It is thus generic that for constitutive models in the form of a stress evolution, the vorticity tends to give rise to a significant first normal stress difference in simple shear. This includes several popular phenomenological models for yield stress fluids^{19,20,52}. (A recent microstructure-based model for dense hard particle suspensions also falls into this class and similarly predicts significant normal stress differences⁵³.) The effect of the vorticity on the first normal stress difference can however still be mitigated in phenomenological models by using large prefactors in front of the stress relaxation term and/or the \mathbf{E}^∞ source term.

Finally, it should be noted that our analysis focuses on the dynamic yield stress tensor. Although it is reasonable to believe that the static stress tensor will not be aligned with \mathbf{E}^∞ if the dynamic one is not, it is also possible that the effect of the vorticity is less pronounced on the former, as static yield occurs after a finite strain of order 0.1 to 1, whereas the dynamic yield stress is measured in the limit of infinite strain.

3.2 Steady flow: extensional vs simple shear

We now turn to steady flow, focusing on simple shear flow ($\alpha = \pi/4$) with rate $\dot{\gamma}$

$$\nabla \mathbf{u}^\infty = \begin{pmatrix} 0 & \dot{\gamma} \\ 0 & 0 \end{pmatrix}, \quad (6)$$

and planar extensional flow ($\alpha = 0$) with rate $\dot{\epsilon}$ (note that $\dot{\epsilon} = \dot{\gamma}/2$)

$$\nabla \mathbf{u}^\infty = \begin{pmatrix} \dot{\epsilon} & 0 \\ 0 & -\dot{\epsilon} \end{pmatrix}. \quad (7)$$

Specifying Eqn (1) for a simple shear, we get

$$\dot{\sigma} = \frac{\kappa - N_1}{2} \dot{\gamma} + \left[\beta - 2\xi \left(N_1^2/4 + \sigma^2 \right) \right] \sigma, \quad (8)$$

$$\dot{N}_1 = 2\dot{\gamma}\sigma + \left[\beta - 2\xi \left(N_1^2/4 + \sigma^2 \right) \right] N_1.$$

Similarly, in planar extension, we get

$$\dot{\sigma} = \left[\beta - 2\xi \left(N_1^2/4 + \sigma^2 \right) \right] \sigma, \quad (9)$$

$$\dot{N}_1 = 2\dot{\epsilon}\kappa + \left[\beta - 2\xi \left(N_1^2/4 + \sigma^2 \right) \right] N_1.$$

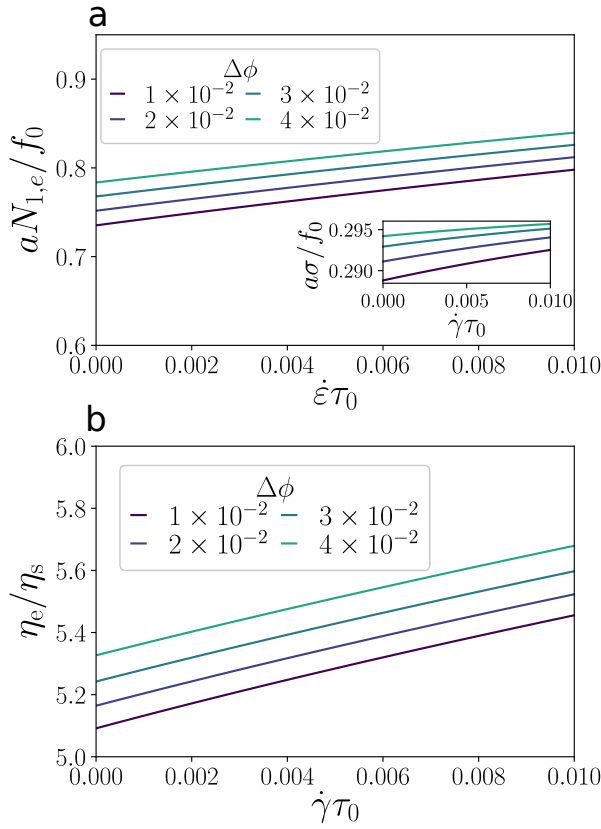


Fig. 3 (a) Flow curves in planar extensional flow ($\alpha = 0$): normal stress difference as a function of the extensional shear rate, for several volume fractions above jamming, labelled by their distance to jamming $\Delta\phi = \phi - \phi_j$. In inset, flow curves in simple shear ($\alpha = \pi/4$), for the same volume fractions. (b) Corresponding Trouton ratio as a function of the applied shear rate.

The steady state flow curves are given by the stable fixed point of these equations. The simple shear case has been exposed in³³, but we replot it in the inset of Fig. 3a, alongside the predicted rheology for extensional flow, to ease the comparison. As already discussed in a previous section, under both deformations the model shows a yield stress, for simple shear on both σ and N_1 , and in extensional flow only on N_1 . Unsurprisingly, by symmetry σ vanishes in steady extensional flow. This can also be seen in Eqn (9), as we always have $[\beta - 2\xi(N_1^2/4 + \sigma^2)] < 0$ above the normal yield stress. None of the flow curves is following a Herschel-Bulkley law, but rather a Bingham law at small shear rates. Indeed, expanding the stable stationary solutions of Eqn (8) for N_1 and σ up to first order in $\dot{\gamma}$, we get the following expression for stationary state under simple shear

$$\sigma = \text{sgn}(\dot{\gamma}) \sigma_{y,s} + \left(\frac{\kappa}{4\beta} - \frac{1}{\kappa\xi} \right) \dot{\gamma} + o(\dot{\gamma}), \quad (10)$$

$$N_1 = N_{y,s} + \frac{2\sigma_y}{\beta} |\dot{\gamma}| + o(\dot{\gamma}), \quad (11)$$

with $N_{y,s} = 2\beta/(\xi\kappa)$ and $\sigma_{y,s} = \sqrt{\beta[1 - 2\beta/(\xi\kappa^2)]}/(2\xi)$. Similarly, from Eqn (9), we get the flow curve at first order under

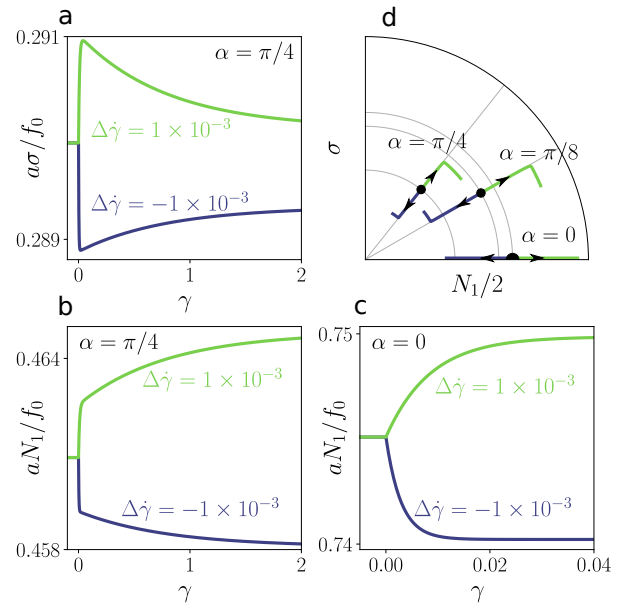


Fig. 4 (a) Shear stress as a function of the applied strain after respectively step increase (green curve) and step decrease (blue curve) of the shear rate, with $\dot{\gamma}_0 \tau_0 = 2 \times 10^{-3}$, $\Delta\dot{\gamma} \tau_0 = \pm 10^{-3}$ and $\Delta\phi = 10^{-2}$, under simple shear. (b) Associated normal stress difference versus strain, under the same conditions as (a). (c) Normal stress difference as a function of the applied strain in planar extensional flow, for otherwise same conditions as in (a)-(b). (d) Schematic trajectories in the $(N_1/2, \sigma)$ plane in simple shear ($\alpha = \pi/4$), planar extension ($\alpha = 0$), and a flow in between ($\alpha = \pi/8$). Overshoots and undershoots for $\alpha \neq 0$ come from the radial dynamics being much faster than the azimuthal one.

planar extension

$$N_1 = 2\text{sgn}(\dot{\epsilon})\tau_c + \frac{\kappa}{\beta}\dot{\epsilon} + o(\dot{\epsilon}). \quad (12)$$

From these curves, we can extract the Trouton ratio predicted by our model. The Trouton ratio for planar extension is defined as $\text{Tr} = \eta_e/\eta_s$, with $\eta_e = (\Sigma'_{11} - \Sigma'_{22})/\dot{\epsilon}$ in planar extension and $\eta_s = \Sigma'_{12}/\dot{\gamma}$ in simple shear, evaluated at $\dot{\gamma} = \dot{\epsilon}$. For a Newtonian fluid, the Trouton ratio takes a value of 4. We show in Fig. 3b that our model predicts a Trouton ratio quite larger than the Newtonian value for soft jammed suspensions. This is another manifestation of the significant rotation of the microstructure and stress tensors under the action of the vorticity in our model. This result stands in contrast with MCT for soft glasses, which predicts a sub-Newtonian Trouton ratio⁵⁴. Experimentally, Trouton ratios significantly larger than the Newtonian value have been observed for uniaxial elongation of concentrated emulsions^{55,56}.

4 Transients

In this section we consider the time evolution of the stress provided in Eqn (1) under time-dependent driving protocols which are commonly explored experimentally.

4.1 Steps in rate: stress overshoot, stress relaxation

We will here focus on the step-in-shear-rate protocol. Starting from a steady state under a shear rate $\dot{\gamma}_0$, one suddenly increases or decreases the applied shear rate to $\dot{\gamma}_0 + \Delta\dot{\gamma}$. For this protocol, it

is convenient to consider the dynamics in polar coordinates S and θ (see Eqn (4)). From Eqn (1), we have

$$\dot{S} = \frac{\dot{\gamma}\kappa}{2} \cos(2\alpha - \theta) + (\beta - 2\xi S^2)S \quad (13)$$

$$\dot{\theta} = \dot{\gamma} \left[\frac{\kappa}{2S} \sin(2\alpha - \theta) - \tan \alpha \right]. \quad (14)$$

As discussed in introduction, in the elastic flow regime S has a much faster dynamics than θ . This is clearly illustrated here by the decompositions $S = S_0 + \delta S$ and $\theta = \theta_0 + \delta\theta$, with S_0 and θ_0 the steady-state values at $\dot{\gamma}_0$. From Eqn (14) we see that right at the step in shear rate $\delta\dot{S} \sim \Delta\dot{\gamma}\tau_0$, whereas $\delta\dot{\theta} = 0$, while just after the increment, $\delta\dot{\theta} \sim \dot{\gamma}\tau_0\delta S/S_0$. We represented this dynamics in the polar plane (S, θ) in Fig. 4d, illustrating the fast radial relaxation and the comparatively slow azimuthal one, irrespective of the value of α (with the exception of $\alpha = 0$, for which the θ dynamics is frozen). From this representation we can easily predict the transients of $\sigma = S \sin \theta$ and $N_1 = 2S \cos \theta$, which we represent in Fig. 4a.

An increase in shear rate ($\Delta\dot{\gamma} > 0$) will trigger a fast increase of S and a slow decrease of θ , leading to an overshoot in σ and a monotonic increase in N_1 . Conversely, a decrease in shear rate ($\Delta\dot{\gamma} < 0$) will lead to an undershoot in σ and a monotonic decrease in N_1 . Integrating the dynamics numerically, we indeed confirm this behavior in Fig. 4a-b for $\alpha = \pi/4$ and $\Delta\dot{\gamma} = \pm 10^{-3}$. Of course the planar extension ($\alpha = 0$) here stands out, as $\sigma = 0$ and the relaxation proceeds only on N_1 and is monotonic, as shown in Fig. 4c.

A particular case of step-change-in-shear-rate is flow cessation, i.e. $\Delta\dot{\gamma} = -\dot{\gamma}_0$. On flow cessation in simple shear the shear stress relaxes down to a finite value, the residual stress σ_r . An intriguing observation is that σ_r is a decreasing function of $\dot{\gamma}_0$; the faster one initially shears, the smaller the residual stress on cessation^{16,29-31}. While this effect may involve a stress-dependent cooperativity in the plasticity (e.g. plastic avalanches), we have shown that it can already be qualitatively reproduced by our model³³. The mechanism can also be easily understood in the polar representation. According to Eqn (14), when the shear is stopped θ is frozen and only S relaxes down to the von Mises yield value $S = \sqrt{\beta/2\xi}$. Because the steady-state value of θ is a decreasing function of the shear rate for any $\alpha > 0$, so is the residual stress $\sigma_r = \sqrt{\beta/2\xi} \sin \theta$. This is true whenever $0 < \alpha < \pi/2$, that is, as long as there is a finite vorticity in presence of finite straining in the flow geometry.

4.2 Imposed stress: creep

We now turn to the behavior under constant applied stress. We follow here the protocol of Ref.²⁹. We first apply a pre-shear under a large shear rate, and then let the stress relax to its residual stress tensor Σ_r under vanishing shear. From this initial state, we perform a shear under constant stress.

The stress component we impose depends on the flow. For simple shear flow, we impose the shear stress, which from Eqn (8)

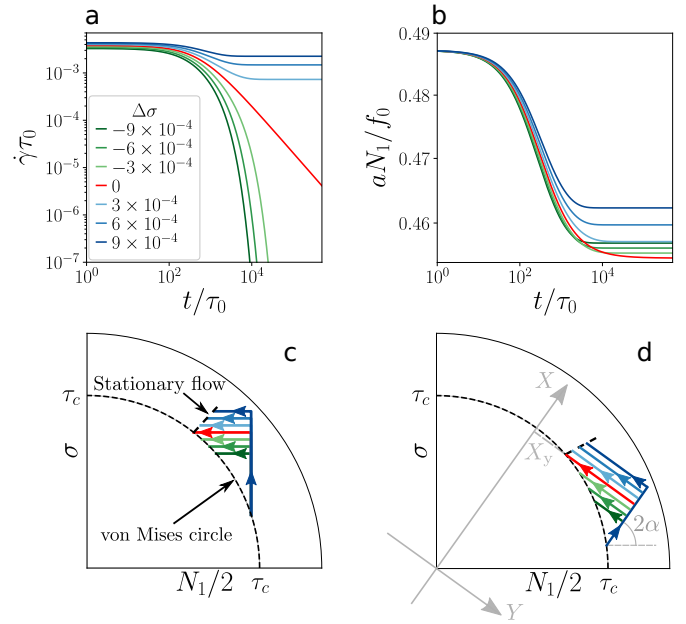


Fig. 5 (a-b) Creep flow in simple shear for several values of imposed shear stresses $\sigma_0 = \sigma_y + \Delta\sigma$, with $\Delta\phi = 0.01$, after a pre-shear under shear rate $\dot{\gamma}_{ps}\tau_0 = 10^{-2}$. Shear rate (a) and normal stress difference (b) as a function of time. (c) Schematic trajectories in the $(N_1/2, \sigma)$ plane for creep in simple shear, showing the origin of the minimum in the long-time normal stress difference as a function of $\Delta\sigma$. (d) Schematic trajectories in the $(N_1/2, \sigma)$ plane for creep under flow with generic α value. Creep corresponds to flow under imposed $X = \Sigma' : \mathbf{E}^\infty / \dot{\gamma}$.

with $\dot{\sigma} = 0$ results in a shear rate

$$\dot{\gamma} = \frac{2\sigma_0}{N_1 - \kappa} \left[\beta - 2\xi \left(N_1^2/4 + \sigma_0^2 \right) \right]. \quad (15)$$

Replacing $\dot{\gamma}$ by its expression in the evolution equation for N_1 , we obtain the following dynamics for N_1 :

$$\dot{N}_1 = \left(\frac{4\sigma_0^2}{N_1 - \kappa} + N_1 \right) \left[\beta - 2\xi \left(N_1^2/4 + \sigma_0^2 \right) \right]. \quad (16)$$

In Fig. 5a, we show numerical integrations of these equations for several values of the imposed shear stress σ , ranging from below to above the simple shear yield stress $\sigma_{y,s}$. Predictably, for $\sigma < \sigma_{y,s}$, the flow halts after a finite time, while for $\sigma > \sigma_{y,s}$ the shear rate decreases towards its finite steady-state value. The normal stress difference N_1 , however, always decays to a finite value, see Fig. 5b. This value is moreover a non-monotonic function of σ taking a minimum for $\sigma = \sigma_{y,s}$. This is most easily understood from the loci of fixed points in the $(N_1/2, \sigma)$ plane, represented in Fig. 5c. For $\sigma < \sigma_{y,s}$, fixed points all lie on the von Mises yield circle ($S = \tau_c$), with an azimuth θ increasing (and thus $N_1 = 2S \cos \theta$ decreasing) with increasing σ . For $\sigma > \sigma_{y,s}$, S increases with σ fast enough to counteract the continuing increase of θ , so that N_1 now increases with σ .

For $\sigma = \sigma_{y,s}$, we get power law decay of the shear rate. A quick look at Eqn (16) reveals that for $\sigma = \sigma_{y,s}$ the fixed point of the N_1 dynamics (located at $N_{1,y,s}$) is marginally stable, so that the late dynamics of $\delta N_1 = N_1 - N_{1,y,s}$ is $\delta\dot{N}_1 \propto -(\delta N_1)^2$. This implies that at late times $\delta N_1 \propto t^{-1}$, which in turn, from Eqn (15) implies that

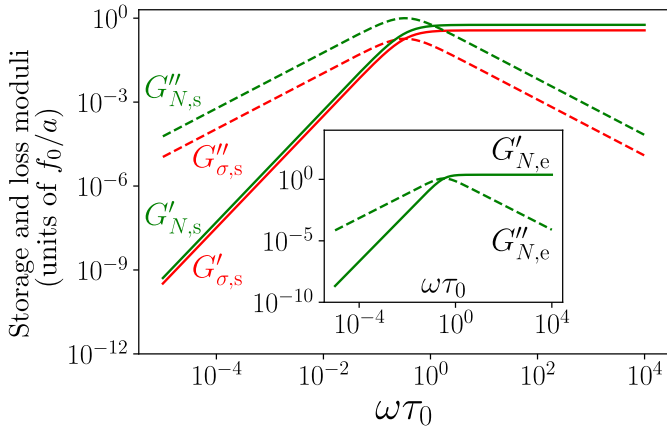


Fig. 6 Frequency dependence of the storage and loss moduli under parallel superposition on the von Mises yield circle in simple shear (main panel) and in planar extension (inset).

the final decay of the shear rate is in $\dot{\gamma} \propto t^{-1}$, which is indeed the exponent we observe in Fig. 5. A power law decay $\dot{\gamma} \propto t^{-b}$ is also observed experimentally^{29,57}, but with $b \approx 2/3$. A recent phenomenological constitutive model showing otherwise good agreement with experimental data on microgels predicts $b = 1/n > 1$, with $n < 1$ the Herschel-Bulkley exponent⁵⁸.

Creep can also be defined for more general flows parametrized by α (see Eqn (2)), as a deformation under constant $X \equiv \boldsymbol{\Sigma}' : \mathbf{E}^\infty / \dot{\gamma}$. The quantity X is the projection of the stress tensor on \mathbf{E}^∞ , and measures the dissipative part of the stress⁵⁹. It reduces to σ in simple shear. In the plane $(N_1/2, \sigma)$, stresses sharing the same X value fall on a line making an angle $2\alpha - \pi/2$ with the horizontal axis, as depicted in Fig. 5d. Creep for arbitrary α follows the same phenomenology than in simple shear. For $X < X_y$, with X_y the yield dissipative stress, the system quickly relaxes towards an arrested state. For $X = X_y$, the shear rate decays at long times as t^{-1} . For $X > X_y$, the system reaches a steady flow. Separately, the non-dissipative part of the stress Y (which we can define as $Y \equiv \sqrt{|\boldsymbol{\Sigma}' - 2X\mathbf{E}^\infty|^2/2}$) relaxes towards a value which is a non-monotonic function of the imposed X , taking a minimum for $X = X_y$.

5 Parallel superposition

The question of the visco-elasticity of flowing soft jammed materials has received some attention recently^{17,32}. In particular, a central question is the quantification of elasticity in yielded suspensions, which are not expected to be purely viscous. We here report the predictions of our constitutive model, Eqn (1), under parallel superposition. We follow a protocol similar to the one of Ref.¹⁷, and apply in simple shear a shear stress with a small oscillation around an averaged value, that is, $\sigma = \bar{\sigma} + \text{Re}(\delta\sigma e^{i\omega t})$ with $\bar{\sigma} > \sigma_{y,s}$. We then measure a response in shear rate $\dot{\gamma} = \bar{\dot{\gamma}} + \text{Re}(i\omega\delta\dot{\gamma}e^{i\omega t})$, and normal stress difference $N_1 = \bar{N}_1 + \text{Re}(\delta N_1 e^{i\omega t})$.

The DC components then satisfy

$$\bar{N}_1 = \frac{\kappa - \sqrt{\kappa^2 - 16\bar{\sigma}^2}}{2} \quad (17)$$

$$\bar{\dot{\gamma}} = \frac{2\bar{\sigma}}{\bar{N}_1 - \kappa} \left[\beta - 2\xi \left(\frac{\bar{N}_1^2}{4} + \bar{\sigma}^2 \right) \right]. \quad (18)$$

Linearizing Eqn (8), one finds that $\delta\dot{\gamma}$, $\delta\sigma$ and δN_1 satisfy

$$\begin{aligned} \left[i\omega + \frac{E_\sigma}{\eta_\sigma} \right] \delta\sigma &= i\omega E_\sigma \delta\dot{\gamma} + C_\sigma \delta N_1, \\ \left[i\omega + \frac{E_N}{\eta_N} \right] \delta N_1 &= i\omega E_N \delta\dot{\gamma} + C_N \delta\sigma, \end{aligned} \quad (19)$$

with effective elastic moduli and viscosities $E_\sigma = (\kappa - \bar{N}_1)/2$, $\eta_\sigma = (\kappa - \bar{N}_1)/[-2\beta + \xi(\bar{N}_1^2 + 12\bar{\sigma}^2)]$, $E_N = 2\bar{\sigma}$ and $\eta_N = 2\bar{\sigma}/[-\beta + \xi(3\bar{N}_1^2/2 + 2\bar{\sigma}^2)]$, and couplings $C_\sigma = -(\bar{\dot{\gamma}}/2 + \xi\bar{N}_1\bar{\sigma})$ and $C_N = (2\bar{\dot{\gamma}} - 4\xi\bar{\sigma}\bar{N}_1)$.

Thus at linear level (Eqn (19)), under parallel superposition our model can be interpreted as a pair of Maxwell models for shear and normal stresses, coupled through C_σ and C_N , only with effective viscosities and elastic moduli which depend on the mean applied stress $\bar{\sigma}$. From Eqn (19), we can get the storage and loss moduli $G'_{\sigma,s} = \text{Re}(\delta\sigma/\delta\dot{\gamma})$ and $G''_{\sigma,s} = \text{Im}(\delta\sigma/\delta\dot{\gamma})$, as well as equivalent moduli for normal stresses $G'_{N,s} = \text{Re}(\delta N_1/\delta\dot{\gamma})$ and $G''_{N,s} = \text{Im}(\delta N_1/\delta\dot{\gamma})$.

These are plotted as a function of frequency at yield, i. e. for $\bar{\sigma} = \sigma_{y,s}$ in Fig. 6. The response is unsurprisingly the one of a Maxwell model, with a material essentially viscous at low frequencies and elastic at high frequencies. Indeed, assuming that $\bar{\sigma} = \sigma_{y,s}$, a short calculation leads to

$$G'_{\sigma,s} = \frac{(\kappa - N_{y,s})\omega^2}{2(\omega^2 + 4\beta^2)}, \quad G''_{\sigma,s} = \frac{(\kappa - N_{y,s})\beta\omega}{\omega^2 + 4\beta^2}, \quad (20)$$

$$G'_{N,s} = \frac{2\sigma_{y,s}\omega^2}{\omega^2 + 4\beta^2}, \quad G''_{N,s} = \frac{4\beta\omega}{\omega^2 + 4\beta^2}. \quad (21)$$

The frequency dependence is not reported in the experimental literature, either because it is not accessible with the employed technique³², or because it is argued to be mild¹⁷.

The same analysis can be carried out in any flow geometry, and for instance we show in the inset of Fig. 6 the visco-elasticity at yield under planar extension, which involves only the storage and loss moduli associated with the normal stress difference

$$G'_{N,e} = \frac{2\kappa\omega^2}{\omega^2 + 4\beta^2}, \quad G''_{N,e} = \frac{4\kappa\beta\omega}{\omega^2 + 4\beta^2}. \quad (22)$$

Coming back to visco-elasticity in simple shear, we show the storage and loss moduli as a function of mean stress $\bar{\sigma}$ for several frequencies in Fig. 7. The storage modulus is in qualitative agreement with experiments, with $G'_{\sigma,s}$ rapidly decreasing just above yield for low frequencies^{17,32}. At low frequencies, the loss modulus decreases with increasing $\bar{\sigma}$, but at higher frequencies (for the volume fraction shown in Fig. 7, for $\omega\tau_0 \gtrsim 5 \times 10^{-1}$), the trend changes and $G''_{\sigma,s}$ becomes an increasing function of $\bar{\sigma}$. Experimentally, Ref.¹⁷ reports a decrease of $G''_{\sigma,s}$ with $\bar{\sigma}$. From the

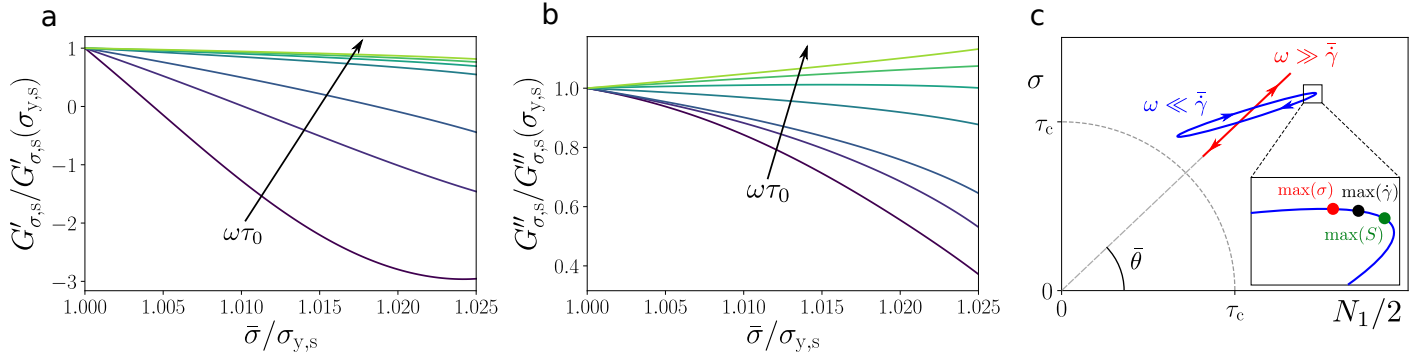


Fig. 7 Storage (a) and loss (b) moduli predicted for a parallel superposition as a function of $\bar{\sigma} \geq \sigma_{y,s}$ in simple shear for $\Delta\phi = 10^{-2}$. Curves from bottom to top correspond to $\omega\tau_0 = 3 \times 10^{-2}, 5 \times 10^{-2}, 8 \times 10^{-2}, 3 \times 10^{-1}, 5 \times 10^{-1}, 7 \times 10^{-1}$, and 1. (c) Schematic trajectories in the $(N_1/2, \sigma)$ plane at high (red segment) and low (blue ellipse) frequencies. In inset, a zoomed in view on the apex of the ellipse followed clockwise at low frequencies, which shows that the maximum of σ occurs before the maximum of $\dot{\gamma}$ (which in turn precedes the maximum of S), giving rise to a negative storage modulus $G'_{\sigma,s}$.

data in Ref. ³², assuming that the coefficients of the Jeffrey model used in this work are frequency independent, we can also infer a decrease of $G'_{\sigma,s}$ with $\bar{\sigma}$, however this decrease gets milder with increasing frequencies. This suggests that the role of frequency is perhaps overlooked in the literature.

An apparently quite surprising result is that the storage modulus $G'_{\sigma,s}$ can become negative when $\bar{\sigma}$ increases. Said otherwise, the suspension seemingly behaves like a visco-elastic fluid with *negative* elastic modulus. To understand this result, it is useful to return to the polar representation of the stress in Eqn (14), where the fact that the dynamics of θ is much slower than the one of S again plays a key role. Introducing $S = \bar{S} + \delta S e^{i\omega t}$ and $\theta = \bar{\theta} + \delta\theta e^{i\omega t}$, δS and $\delta\theta$ follow

$$\begin{aligned} [i\omega - \beta + 6\xi\bar{S}^2] \delta S &= i\omega \frac{\kappa \sin \bar{\theta}}{2} \delta\gamma + \frac{\bar{\gamma}\kappa \cos \bar{\theta}}{2} \delta\theta \\ [i\omega + \bar{\gamma} \frac{\kappa}{2\bar{S}} \sin \bar{\theta}] \delta\theta &= -\frac{\bar{\gamma}\kappa \cos \bar{\theta}}{2\bar{S}^2} \delta S \end{aligned} \quad (23)$$

We sketch in Fig. 7c the dynamics in the (S, θ) plane under the two opposite regimes $\omega/\bar{\gamma} \ll 1$ and $\omega/\bar{\gamma} \gg 1$. Under oscillatory shear at large frequencies $\omega/\bar{\gamma} \gg 1$, we can neglect the terms involving $\bar{\gamma}$ in Eqn (23). We thus notice that θ is essentially frozen, and S follows a usual Maxwell model

$$\left(i\omega + \frac{E_S}{\eta_S} \right) \delta S = i\omega E_S \delta\gamma, \quad (24)$$

with effective elastic modulus and viscosity

$$E_S = \frac{\kappa \sin \bar{\theta}}{2} > 0, \quad \eta_S = \frac{\kappa \sin \bar{\theta}}{-2\beta + 12\xi\bar{S}^2} > 0. \quad (25)$$

To determine the sign of η_S , we used that $-2\beta + 12\xi\bar{S}^2 > -2\beta + 12\xi\tau_c^2 = 4\beta > 0$. In this limit the system thus follows a radial oscillation in the (S, θ) plane, such that $\delta\sigma$ is in phase with δS , leading to a positive $G'_{\sigma,s}$.

In the $\omega \ll \bar{\gamma}$ regime, at linear order in ω the S response in Eqn (23) is still an effective Maxwell model, now with effective

elastic modulus and viscosity

$$E_S = \frac{\kappa \sin \bar{\theta}}{2 [1 - (\tan \bar{\theta})^{-2}]}, \quad \eta_S = \frac{\kappa \sin \bar{\theta}}{-2\beta + 12\xi\bar{S}^2 + \frac{\bar{\gamma}\kappa}{\bar{S}} \cos \bar{\theta}} > 0. \quad (26)$$

Now, $E_S > 0$ if $\bar{\theta} > \pi/4$, which is fulfilled within our model for small shear rates as $\cos \theta_y = \kappa\sqrt{2\beta/\xi} > 1/\sqrt{2}$ for volume fractions close to jamming. S therefore still responds like a usual visco-elastic variable, with positive storage modulus. However, now θ also oscillates, so that in the (S, θ) plane, the system follows an elongated ellipse. According to the second line of Eqn (23), $\delta\theta$ is almost in phase opposition with δS , but not quite: S reaches its maximum slightly before θ hits its minimum point, the phase difference differing from π by an angle of order $\omega/\bar{\gamma}$. This implies that the ellipse is followed in a clockwise manner. This in turn implies that σ reaches its maximum slightly before S does, as can be easily understood from the inset of Fig. 7c. More precisely, using $\delta\sigma = \sin \bar{\theta} \delta S + \cos \bar{\theta} \bar{S} \delta\theta$, we have

$$\delta\sigma = \left(\frac{-\cos 2\bar{\theta}}{\cos \bar{\theta}} + \frac{2i\omega}{\bar{\gamma}\kappa \tan \bar{\theta}} \right) \frac{\delta S}{\tan \bar{\theta}} \quad (27)$$

which shows that the phase difference between δS and $\delta\sigma$ is also of order $\omega/\bar{\gamma}$. It turns out that the values of $\bar{\theta}$ and κ are such that the phase advance of $\delta\sigma$ on δS is actually large enough to make the phase difference between $\delta\sigma$ and $\delta\gamma$ larger than $\pi/2$, which corresponds to a negative storage modulus $G'_{\sigma,s}$.

Physically, the situation is thus clear. Strain rate oscillations induce both an oscillation in the overlap between particles in contact, but also in the orientation of these contacts because of the vorticity. The negative storage modulus observed under flow is just a consequence of the oscillation of the principal axes of the microstructure under slow enough oscillatory driving, and more specifically of the small lag of the orientation of the contact with respect to the oscillation of the overlaps.

Our model thus offers a simple physical picture for the collapse of the storage modulus just above yield^{17,32}, which differs significantly from the naive interpretation of a loss of elastic network, which is difficult to believe in a concentrated soft suspension above the jamming volume fraction. It is actually much more

plausible that the storage modulus becomes negative because of the rotation of the microstructure in near-antiphase with the driving oscillation, in a system with otherwise essentially intact elastic integrity (and this despite the contacts making up the elastic backbone being constantly renewed by the flow). Once again, measuring the frequency dependence of the visco-elastic moduli seems essential in order to test these ideas in experiments.

Finally, let us remark that a very similar phenomenology is actually observed in polymer solutions^{60–62}, with a negative storage modulus at low frequencies, and a simple tensorial Maxwell model including the vorticity in a frame-indifferent manner is known to recover qualitatively the behavior⁶³.

6 Conclusions

We have shown that, within a constitutive model recently derived from microscopic dynamics, many aspects of the steady and transient rheology of concentrated soft suspensions (the von Mises yield criterion, the Trouton ratio, viscoelasticity in flow and transients under steps in shear rate or shear stress) depend strongly on the interplay between the elastic relaxation of the microstructure and advection. In particular the vorticity leads to significant misalignment of the microstructure (characterized by a fabric tensor) with respect to the strain rate tensor. This in turn leads to a strong deviation from the quasi-Newtonian behavior often assumed in the literature^{2,22,24,26,64}. This calls for renewed efforts to measure experimentally normal stress differences, in particular the first normal stress difference (the one affected by the vorticity) in simple shear. Only few pioneering works address this issue, but a consensus remains to emerge, the first normal stress difference being either found positive and much smaller than the shear stress^{15,65} or on the contrary negative and as large if not larger in amplitude than the shear stress^{27,28}.

If such consensus does not exist, in the sense that normal stresses are found very much material dependent, or if the consensus is that actually normal stresses are small under simple shear, it would imply that the vorticity, which appears in a prescribed, non-negotiable manner in tensorial stress evolution because of frame indifference, is not the dominant contributor to the orientation of the fabric and/or stress. This situation is also seen for suspensions of non-Brownian hard particles below their jamming point, where the first normal stress difference is known to be small compared to the shear stress⁶⁶. Frame-indifferent stress evolution models unsurprisingly tend to overestimate it^{53,67,68}, though this is not always the case, as some phenomenological models give good predictions, with careful adjustments of key parameters^{69–71}. Looking at how the predictions depend on said parameter values, we see that both Phan-Thien^{69,70} and Ozenda et al.⁷¹ find a large sensitivity of the first normal stress difference on the parameter governing the strength of the stress or fabric relaxation, corresponding to $[\beta(\phi) - \xi(\phi)\mathbf{\Sigma}' : \mathbf{\Sigma}']$ in Eqn (1). This is consistent with the idea that elastic relaxation must remain dominant over the rotation due to the vorticity for the first normal stress difference to remain small. This points to possible guidelines for improving the closures involved in the derivation of our model, if needed.

Interestingly, concentrated Brownian suspensions below jam-

ming show a negative value of N_1 in simple shear, associated with a microstructure anisotropy misaligned from the principal axis of the strain-rate tensor, only in a direction opposite to the vorticity^{72–74}. A careful analysis of the origin of this counter-rotation reveals that the microstructure is bimodal, with two directions for near-interactions accumulations. The first one lies between the compressional and flow gradient axes (as expected from a rotation by the vorticity), but the second one is along the flow direction, and corresponds to the increased probability of having particles following each other along streamlines^{73,74}. In concentrated systems under simple shear, this flow ordering takes over the statistics of near interactions and yields the apparent counter-rotation of the second moment of the microstructure. An approach based on a fabric tensor such as ours cannot capture a bimodal microstructure, which requires at least a fourth-ranked tensor descriptor⁶⁸. Nonetheless, it is unclear at this stage if a similar phenomenon occurs for soft jammed suspensions. A contact accumulation along the flow direction may be observed in a jammed microgel suspension, especially during flow cessation transients¹⁶, but N_1 is found positive in the same system⁸, indicating that flow-aligned contacts may not play a crucial role in the rheology, perhaps because they carry lower forces than contacts closer to the compression or gradient directions.

At a more fundamental level, it is remarkable that our constitutive model, which is based on assumptions of well-developed, homogeneous flow, can capture at least qualitatively many non-trivial aspects of the rheology of soft jammed suspensions usually attributed to possibly more complex or at least conceptually quite different microscopic mechanisms such as localized plastic events or spatial cooperativity. Of course it is entirely possible that these mechanisms, once coarse-grained, give rise to a stress evolution equation structurally close to Eqn (1) (and indeed Hand theory⁷⁵ would argue for any constitutive model to be generically resembling Eqn (1)). It would then not be a surprise that such equation would give qualitatively similar predictions to ours, and to some extent this would prevent the possibility to decide what is the right microscopic picture from macroscopic measurements. This calls for more precise measurements of microstructural aspects of soft suspensions under flow, in experiments and numerical simulations, in order to guide further theoretical developments.

Conflicts of interest

There are no conflicts to declare.

Acknowledgements

This work is supported by the French National Research Agency in the framework of the "Investissements d'avenir" program (ANR-15-IDEX-02). We thank Morton Denn for pointing out to us the polymer solution literature on negative storage modulus in parallel superposition.

Appendix A: main steps of the derivation of the stress evolution equation

We sketch in this Appendix the key steps of the derivation of the stress evolution equation, Eqn (1). More details can be found in

Ref.^{33,34}. The starting point is the exact evolution equation for the pair correlation function $g(\mathbf{r})$, which reads as

$$\begin{aligned} \partial_t g(\mathbf{r}) + \nabla \cdot \left[(\nabla \mathbf{u}^\infty \cdot \mathbf{r}) g(\mathbf{r}) - \mathbf{F}(\mathbf{r}) g(\mathbf{r}) \right. \\ \left. - \rho \int \mathbf{F}(\mathbf{r}') g_3(\mathbf{r}, \mathbf{r}') d\mathbf{r}' \right] = 0, \end{aligned} \quad (28)$$

Eqn (28) is not closed in terms of $g(\mathbf{r})$, but also involves the three-body correlation function $g_3(\mathbf{r}, \mathbf{r}')$. Defining the particle stress tensor Σ from the virial formula⁷⁶ as

$$\Sigma = \frac{\rho^2}{2} \int (\mathbf{r} \otimes \mathbf{F}(\mathbf{r})) g(\mathbf{r}) d\mathbf{r}, \quad (29)$$

one can obtain an evolution equation for the stress tensor by multiplying Eqn (28) by $\frac{1}{2}\rho^2 \mathbf{r} \otimes \mathbf{F}(\mathbf{r})$ and integrating over \mathbf{r} . One then finds

$$\dot{\Sigma} = \nabla \mathbf{u}^\infty \cdot \Sigma + \Sigma \cdot \nabla \mathbf{u}^{\infty T} + \mathbf{H}_2 - \mathbf{H}_3 \quad (30)$$

where the tensors \mathbf{H}_2 and \mathbf{H}_3 are defined by integrals over the pair and three-body correlation functions respectively,

$$\begin{aligned} \mathbf{H}_2 = \frac{\rho^2}{2} \int [(\mathbf{E}^\infty : \mathbf{e}_r \otimes \mathbf{e}_r) ((\mathbf{r} \otimes \mathbf{r}) \cdot \nabla \mathbf{F}(\mathbf{r}) - \mathbf{r} \otimes \mathbf{F}(\mathbf{r})) \\ - \mathbf{F}(\mathbf{r}) \otimes \mathbf{F}(\mathbf{r}) - (\mathbf{r} \otimes \mathbf{F}(\mathbf{r})) \cdot \nabla \mathbf{F}(\mathbf{r})^T] g(\mathbf{r}) d\mathbf{r}, \end{aligned} \quad (31)$$

$$\begin{aligned} \mathbf{H}_3 = \frac{\rho^3}{2} \iint [\mathbf{F}(\mathbf{r}') \otimes \mathbf{F}(\mathbf{r}) + (\mathbf{r} \otimes \mathbf{F}(\mathbf{r}')) \cdot \nabla \mathbf{F}(\mathbf{r})^T] \\ \times g_3(\mathbf{r}, \mathbf{r}') d\mathbf{r} d\mathbf{r}'. \end{aligned} \quad (32)$$

A corresponding evolution equation for the deviatoric part Σ' of the stress tensor is obtained by taking the deviatoric part of Eqn (30). However, the resulting equation is not closed in terms of Σ' . The closed equation Eqn (1) is then obtained after a set of approximations, as detailed in Ref.^{33,34}. (i) The three-body correlation function $g_3(\mathbf{r}, \mathbf{r}')$ is expressed in terms of the pair correlation function $g(\mathbf{r})$ through the Kirkwood approximation,

$$g_3(\mathbf{r}, \mathbf{r}') \approx g(\mathbf{r})g(\mathbf{r}')g(\mathbf{r} - \mathbf{r}'). \quad (33)$$

(Other choices are possible, see for instance^{43,77}.) (ii) The anisotropic part of the pair correlation function is expanded to lowest order, that is to the second harmonic. (iii) The isotropic part of the pair correlation is given a schematic form with an infinitely thin peak for the first neighbor shell, and a uniform sea of particles for larger distances; this simplified form can be parametrized only in terms of the pressure. (iv) The pressure, whose evolution equation is obtained by taking the trace of Eqn (30), turns out to be a fast dynamical variable and can be eliminated using an equation of state $p(\phi)$, where ϕ is the surface fraction of particles.

Appendix B: strain rate for generic 2D flow

We here briefly show the origin of our scalar parametrization Eqn (2). In the main text, we presented in Eqn (2) a scalar parametrization of a steady uniform 2D flow. For a generic 2D flow (possibly unsteady and non uniform), a generalization of this

parametrization is useful only if it is frame-indifferent, that is, the scalar characterizing the flow is invariant under a time dependent rotation of the flow^{59,78}. Generically, a flow is characterized by its local velocity gradient $\nabla \mathbf{u}^\infty$. The velocity gradient itself is not frame-indifferent, because its antisymmetric part, the vorticity, is not. One should thus not parametrize the velocity gradient, but only its frame-indifferent bit, defined as follows^{59,78}

$$(\nabla \mathbf{u}^\infty)' = \nabla \mathbf{u}^\infty - \Omega_{\text{SR}}^\infty, \quad (34)$$

where $\Omega_{\text{SR}}^\infty$ is the local spin tensor of the eigenvectors of \mathbf{E}^∞ , that is, the part of the total spin Ω^∞ which corresponds to a local solid rotation. Said otherwise, the frame indifferent part of the local velocity gradient is the velocity gradient in a frame in which the local strain rate tensor does not rotate. The spin tensor $\Omega_{\text{SR}}^\infty$ is defined as $\Omega_{\text{SR}}^\infty \cdot \mathbf{x} = \boldsymbol{\omega} \times \mathbf{x}$ for any vector \mathbf{x} , with⁷⁸

$$\boldsymbol{\omega} = \mathbf{e} \times \left(\frac{\partial \mathbf{e}}{\partial t} + \mathbf{u}^\infty \cdot \nabla \mathbf{e} \right), \quad (35)$$

with $\mathbf{e} = \mathbf{e}_1, \mathbf{e}_2$, one of the unit eigenvectors of \mathbf{E}^∞ (these eigenvectors are orthogonal, such that they share the same spin.) From this we can define a frame-indifferent flow shape $\mathbf{K}^\infty = (\nabla \mathbf{u}^\infty)' / \sqrt{(\nabla \mathbf{u}^\infty)' : (\nabla \mathbf{u}^\infty)'}$. (For the special case of steady uniform flows considered in the main text $(\nabla \mathbf{u}^\infty)' = \nabla \mathbf{u}^\infty$, and thus $\mathbf{K}^\infty = \nabla \mathbf{u}^\infty / \sqrt{\nabla \mathbf{u}^\infty : \nabla \mathbf{u}^\infty}$.)

The set of possible 2D flows of course include planar extension and simple shear. We look for parametrization following the usual conventions for the principal axes of these two specific flows, corresponding for planar extension to

$$\mathbf{K}^\infty = \begin{pmatrix} 1/\sqrt{2} & 0 \\ 0 & -1/\sqrt{2} \end{pmatrix}, \quad (36)$$

and for simple shear to

$$\mathbf{K}^\infty = \begin{pmatrix} 0 & 1 \\ 0 & 0 \end{pmatrix}. \quad (37)$$

We can generically express \mathbf{K}^∞ in terms of the eigenvectors of \mathbf{E}^∞ ,

$$\mathbf{K}^\infty = a\mathbf{e}_1 \otimes \mathbf{e}_1 + b\mathbf{e}_2 \otimes \mathbf{e}_2 + c\mathbf{e}_1 \otimes \mathbf{e}_2 + d\mathbf{e}_2 \otimes \mathbf{e}_1, \quad (38)$$

with a, b, c and d four scalars. Now, because of incompressibility \mathbf{K}^∞ is traceless, which imposes $a = -b$. Furthermore, \mathbf{e}_1 and \mathbf{e}_2 are eigenvectors of \mathbf{E}^∞ , which implies that they must also be eigenvectors of the symmetric part of \mathbf{K}^∞ . A quick calculation concludes that this imposes $c = -d$. Finally, $\mathbf{K}^\infty : \mathbf{K}^\infty = 1$, which implies that we can parametrize \mathbf{K}^∞ with an angle α as

$$\mathbf{K}^\infty = \frac{1}{\sqrt{2}} [\cos \alpha (\mathbf{e}_1 \otimes \mathbf{e}_1 - \mathbf{e}_2 \otimes \mathbf{e}_2) + \sin \alpha (\mathbf{e}_1 \otimes \mathbf{e}_2 - \mathbf{e}_2 \otimes \mathbf{e}_1)]. \quad (39)$$

By identification, planar extension corresponds to $\alpha = 0$, and simple shear to $\alpha = \pi/4$. The simplest family of flow shapes that interpolates between the convention Eqn (36) for planar extension in $\alpha = 0$ and the convention Eqn (37) for simple shear in $\alpha = \pi/4$ is a family in which the eigenvectors of \mathbf{E}^∞ are rotated by α with respect to the x - y axes. In the x - y basis, this family

corresponds Eqn (2) in the main text.

Notes and references

- 1 R. T. Bonnecaze and M. Cloitre, in *High Solid Dispersions*, ed. M. Cloitre, Springer Berlin Heidelberg, Berlin, Heidelberg, 2010, pp. 117–161.
- 2 P. Coussot, *Journal of Non-Newtonian Fluid Mechanics*, 2014, **211**, 31–49.
- 3 T. Divoux, D. Tamarii, C. Barentin and S. Manneville, *Physical Review Letters*, 2010, **104**, 208301.
- 4 T. Divoux, C. Barentin and S. Manneville, *Soft Matter*, 2011, **7**, 9335–9349.
- 5 J. M. Piau, *Journal of Non-Newtonian Fluid Mechanics*, 2007, **144**, 1–29.
- 6 P. Møller, A. Fall, V. Chikkadi, D. Derks and D. Bonn, *Philosophical Transactions of the Royal Society A: Mathematical, Physical and Engineering Sciences*, 2009, **367**, 5139–5155.
- 7 J. R. Seth, L. Mohan, C. Locatelli-Champagne, M. Cloitre and R. T. Bonnecaze, *Nature Materials*, 2011, **10**, 838–843.
- 8 T. Liu, F. Khabaz, R. T. Bonnecaze and M. Cloitre, *Soft Matter*, 2018, **14**, 7064–7074.
- 9 P. Partal, A. Guerrero, M. Berjano and C. Gallegos, *Journal of Food Engineering*, 1999, **41**, 33–41.
- 10 A. P. Batista, A. Raymundo, I. Sousa, J. Empis and J. M. Franco, *Food Biophysics*, 2006, **1**, 216–227.
- 11 P. Coussot, L. Tocquer, C. Lanos and G. Ovarlez, *Journal of Non-Newtonian Fluid Mechanics*, 2009, **158**, 85–90.
- 12 M. Dinkgreve, J. Paredes, M. M. Denn and D. Bonn, *Journal of Non-Newtonian Fluid Mechanics*, 2016, **238**, 233–241.
- 13 E. Younes, M. Himl, Z. Stary, V. Bertola and T. Burghelea, *Journal of Non-Newtonian Fluid Mechanics*, 2020, **281**, 104315.
- 14 F. Khabaz, B. F. Di Dio, M. Cloitre and R. T. Bonnecaze, *Journal of Rheology*, 2021, **65**, 241–255.
- 15 H. de Cagny, M. Fazilati, M. Habibi, M. M. Denn and D. Bonn, *Journal of Rheology*, 2019, **63**, 285–290.
- 16 L. Mohan, R. T. Bonnecaze and M. Cloitre, *Physical Review Letters*, 2013, **111**, 268301.
- 17 E. N’Gouamba, J. Goyon and P. Coussot, *Physical Review Fluids*, 2019, **4**, 123301.
- 18 J. G. Oldroyd, *Mathematical Proceedings of the Cambridge Philosophical Society*, 1947, **43**, 100–105.
- 19 P. Saramito, *Journal of Non-Newtonian Fluid Mechanics*, 2007, **145**, 1–14.
- 20 P. Saramito, *Journal of Non-Newtonian Fluid Mechanics*, 2009, **158**, 154–161.
- 21 N. J. Balmforth, I. A. Frigaard and G. Ovarlez, *Annual Review of Fluid Mechanics*, 2014, **46**, 121–146.
- 22 G. Ovarlez, Q. Barral and P. Coussot, *Nature Materials*, 2010, **9**, 115–119.
- 23 G. German and V. Bertola, *Physics of Fluids*, 2010, **22**, 033101.
- 24 A. Shaukat, M. Kaushal, A. Sharma and Y. M. Joshi, *Soft Matter*, 2012, **8**, 10107–10114.
- 25 L. Martinie, H. Buggisch and N. Willenbacher, *Journal of Rheology*, 2013, **57**, 627–646.
- 26 X. Zhang, O. Fadoul, E. Lorenceau and P. Coussot, *Physical Review Letters*, 2018, **120**, 048001.
- 27 R. L. Thompson, L. U. R. Sica and P. R. de Souza Mendes, *Journal of Non-Newtonian Fluid Mechanics*, 2018, **261**, 211–219.
- 28 R. L. Thompson and P. R. de Souza Mendes, *Journal of Rheology*, 2020, **64**, 615–624.
- 29 P. Lidon, L. Villa and S. Manneville, *Rheologica Acta*, 2017, **56**, 307–323.
- 30 L. Mohan, M. Cloitre and R. T. Bonnecaze, *Journal of Rheology*, 2014, **59**, 63–84.
- 31 V. V. Vasisht, P. Chaudhuri and K. Martens, *arXiv:2108.12782 [cond-mat]*, 2021.
- 32 G. Benmouffok-Benbelkacem, F. Caton, C. Baravian and S. Skali-Lami, *Rheologica Acta*, 2010, **49**, 305–314.
- 33 N. Cuny, R. Mari and E. Bertin, *Physical Review Letters*, 2021, **127**, 218003.
- 34 N. Cuny, R. Mari and E. Bertin, preprint arXiv:2102.05524.
- 35 D. J. Durian, *Physical Review Letters*, 1995, **75**, 4780–4783.
- 36 A. Ikeda, L. Berthier and P. Sollich, *Physical Review Letters*, 2012, **109**, 018301.
- 37 D. Vågberg, Y. Wu, P. Olsson and S. Teitel, *Physical Review E*, 2014, **89**, 022201.
- 38 A. Nicolas, E. E. Ferrero, K. Martens and J.-L. Barrat, *Reviews of Modern Physics*, 2018, **90**, 045006.
- 39 E. Lerner, G. Düring and M. Wyart, *Proceedings of the National Academy of Sciences*, 2012, **109**, 4798–4803.
- 40 W. B. Russel, *Journal of Fluid Mechanics*, 1978, **85**, 209–232.
- 41 B. U. Felderhof, *Physica A: Statistical Mechanics and its Applications*, 1983, **118**, 69–78.
- 42 J. F. Brady, *The Journal of Chemical Physics*, 1993, **99**, 567–581.
- 43 E. Nazockdast and J. F. Morris, *Journal of Fluid Mechanics*, 2012, **713**, 420–452.
- 44 S. Varchanis, S. J. Haward, C. C. Hopkins, A. Syrakos, A. Q. Shen, Y. Dimakopoulos and J. Tsamopoulos, *Proceedings of the National Academy of Sciences*, 2020, **117**, 12611–12617.
- 45 C. J. Dimitriou and G. H. McKinley, *Journal of Non-Newtonian Fluid Mechanics*, 2019, **265**, 116–132.
- 46 P. Saramito, *Journal of Non-Newtonian Fluid Mechanics*, 2021, **294**, 104584.
- 47 J. M. Brader, T. Voigtmann, M. Fuchs, R. G. Larson and M. E. Cates, *Proceedings of the National Academy of Sciences*, 2009, **106**, 15186–15191.
- 48 P. Coussot and F. Gaulard, *Physical Review E*, 2005, **72**, 031409.
- 49 M. Castro, D. W. Giles, C. W. Macosko and T. Moaddel, *Journal of Rheology*, 2010, **54**, 81–94.
- 50 P. Saramito and A. Wachs, *Rheologica Acta*, 2017, **56**, 211–230.
- 51 W. Noll, *Indiana University Mathematics Journal*, 1955, **4**, 3–81.

- 52 V. Dansereau, J. Weiss and P. Saramito, Challenges and Innovations in Geomechanics, Cham, 2021, pp. 125–139.
- 53 J. J. J. Gillissen, C. Ness, J. D. Peterson, H. J. Wilson and M. E. Cates, *Physical Review Letters*, 2019, **123**, 214504.
- 54 J. M. Brader, M. E. Cates and M. Fuchs, *Physical Review Letters*, 2008, **101**, 138301.
- 55 M. R. Anklam, G. G. Warr and R. K. Prud'homme, *Journal of Rheology*, 1994, **38**, 797–810.
- 56 S. Rózańska, J. Rózański, M. Ochowiak and P. T. Mitkowski, *Brazilian Journal of Chemical Engineering*, 2014, **31**, 47–55.
- 57 T. Divoux, C. Barentin and S. Manneville, *Soft Matter*, 2011, **7**, 8409–8418.
- 58 K. Kamani, G. J. Donley and S. A. Rogers, *Physical Review Letters*, 2021, **126**, 218002.
- 59 G. G. Giusteri and R. Seto, *Journal of Rheology*, 2018, **62**, 713–723.
- 60 H. C. Booij, *Rheologica Acta*, 1966, **5**, 215–221.
- 61 T. Kataoka and S. Ueda, *Journal of Polymer Science Part A-2: Polymer Physics*, 1969, **7**, 475–481.
- 62 I. F. Macdonald, *Transactions of the Society of Rheology*, 1973, **17**, 537–555.
- 63 H. C. Booij, *Rheologica Acta*, 1966, **5**, 222–227.
- 64 R. A. Basterfield, C. J. Lawrence and M. J. Adams, *Chemical Engineering Science*, 2005, **60**, 2599–2607.
- 65 M. Habibi, M. Dinkgreve, J. Paredes, M. Denn and D. Bonn, *Journal of Non-Newtonian Fluid Mechanics*, 2016, **238**, 33–43.
- 66 M. M. Denn and J. F. Morris, *Annual Review of Chemical and Biomolecular Engineering*, 2014, **5**, 203–228.
- 67 J. D. Goddard, *Journal of Fluid Mechanics*, 2006, **568**, 1–17.
- 68 R. N. Chacko, R. Mari, S. M. Fielding and M. E. Cates, *Journal of Fluid Mechanics*, 2018, **847**, 700–734.
- 69 N. Phan-Thien, *Journal of Rheology (1978-present)*, 1995, **39**, 679–695.
- 70 N. Phan-Thien, X.-J. Fan and B. C. Khoo, *Rheologica Acta*, 1999, **38**, 297–304.
- 71 O. Ozenda, P. Saramito and G. Chambon, *Journal of Fluid Mechanics*, 2020, **898**, A25.
- 72 D. R. Foss and J. F. Brady, *Journal of Fluid Mechanics*, 2000, **407**, 167–200.
- 73 J. F. Morris and B. Katyal, *Physics of Fluids*, 2002, **14**, 1920–1937.
- 74 E. Nazockdast and J. F. Morris, *Physics of Fluids (1994-present)*, 2013, **25**, 070601.
- 75 G. L. Hand, *Journal of Fluid Mechanics*, 1962, **13**, 33–46.
- 76 F. Nicot, N. Hadda, M. Guessasma, J. Fortin and O. Millet, *International Journal of Solids and Structures*, 2013, **50**, 2508–2517.
- 77 J. T. Jenkins, R. Seto and L. L. Ragione, *Journal of Fluid Mechanics*, 2021, **912**, A27.
- 78 P. R. Schunk and L. E. Scriven, *Journal of Rheology*, 1990, **34**, 1085–1119.